Application and Optimization of PML ABC for the 3-D Wave Equation in the Time Domain

Yotka S. Rickard, *Member, IEEE*, Natalia K. Georgieva, *Member, IEEE*, and Wei-Ping Huang, *Senior Member, IEEE*

***Abstract*—A three-dimensional algorithm with the perfectly matched layer (PML) absorbing boundary condition (ABC) for the scalar wave equation in the time domain is presented for general inhomogeneous lossy or loss-free problems. The proposed PML ABC is applicable to practical finite difference schemes treating the time-domain wave equation, such as the time-domain wave-potential (TDWP) technique and the time-domain scalar wave equation approaches to the analysis of optical structures. The time-domain wave equation for lossy media is expressed in terms of stretched coordinate variables. The algorithm is tested for homogeneous and inhomogeneous media. We demonstrate applications to open (radiation) problems and to port terminations in high-frequency circuit problems. New PML conductivity profiles are developed for use with the second order wave equation, which offer lower reflections in a wider frequency band in comparison with the commonly used (in finite-difference time-domain (FDTD) algorithms) profiles. The effect of the termination walls on the overall PML performance is studied and the best choices are singled out.**

***Index Terms*—Absorbing boundary conditions (ABC), finite-difference time-domain (FDTD) methods, perfectly matched layer (PML), wave equation (WE).**

I. Introduction

THE perfectly matched layer (PML) introduced by Berenger [1] is widely accepted as an efficient numerical absorber used in time-domain electromagnetic (EM) solvers. In the time domain, it has been used mainly in conjunction with the finite difference time-domain (FDTD) algorithm to the solution of Maxwell's equations, as well as with the finite element time-domain (FETD) method. PML absorbing boundary conditions (ABCs) have been also developed for most of the frequency-domain techniques, such as the finite element method (FEM) [3], [4] the finite-difference frequency-domain (FDFD) method [5], or the frequency-domain beam propagation method (BPM) [6], [7].

Recent trends in computational electrodynamics include the development of scalar or vector wave equation techniques for applications in numerical algorithms not only for optical waveguides and devices but also in the microwave and millimeter-wave structure analysis. The time-domain vector-potential technique [8] is based on the solution of the vector wave equation for the magnetic vector potential $\vec{A}$. The time-domain wave-potential (TDWP) approach [9], [10] is a novel technique, which uses two scalar quantities, the magnitudes of a pair of collinear vector potentials $(A, F)\hat{\xi}$, in order to analyze an EM problem in a region of distinguished axis $\hat{\xi}$ parallel to the vector potentials. The propagation of the two potential functions is governed by the three-dimensional (3-D) scalar wave equation. Coupling between the wave potentials A and F occurs in the following cases: conducting edges, which are not parallel to $\hat{\xi}$; and material interfaces whose normal is not parallel to $\hat{\xi}$. The current TDWP algorithm takes care of the TE_ξ and TM_ξ mode coupling by domain subdivision and mode transition formulas at the mutual boundaries of the domains [9]. The direction of the VP pair $(A, F)\hat{\xi}$ in each domain is chosen so that coupling between its wave potentials is avoided. Thus, when a domain is terminated by an ABC, there is no coupling to account for but just two wave equations (for A and for F) which are complemented by identical PML absorbers.

In photonics, approaches based on the time domain wave equations are used to analyze optical waveguide problems. Among those, the most widely used are the methods based on the time-domain scalar or semivectorial finite-difference wave equation [11]; as well as the time-domain beam propagation method (BPM) (see, for example, [14]). These techniques would typically reduce the problem to a set of two-dimensional (2-D) scalar wave equations, where one of the dimensions is along the direction of propagation.

These new algorithms require a reliable and efficient ABC, which can handle both open problems (i.e., radiation and scattering) and problems involving port terminations (high-frequency circuit problems). It will become clear from the derivations to follow that the PML ABC proposed in this paper is not limited to electromagnetic problems only. It can be applied to any physical phenomenon modeled by the general lossy 3-D scalar wave equation, which requires reflection-free boundaries.

Recently, the one-directional PML ABC has been applied to terminate one of the ports in a dielectric-slab waveguide problem solved in terms of the 2-D scalar wave equation in the time domain [15]. In this paper, we extend the method proposed in [15] to a general 3-D PML for the 3-D wave equation in the time domain in loss-free or lossy media. To the authors' knowledge, this is the first PML ABC developed and successfully implemented in conjunction with the 3-D wave equation in the time domain. The derivation of the PML equations is based on the well-known stretched-coordinate approach [16].

This paper has three main contributions. We derive the PML formulas of the 3-D scalar wave equation absorber, and discretize them according to the requirements of a finite difference time-domain scheme. We propose modified profiles of the PML variables, which have superior performance (lower reflections in a broader frequency band) in comparison with commonly

Manuscript received October 1, 2001; revised December 10, 2001.

The authors are with the Department of Electrical and Computer Engineering, McMaster University, Hamilton, ON L8S 4K1, Canada.

Digital Object Identifier 10.1109/TAP.2003.809093

used PML profiles when applied to the wave equation absorber. We investigate the influence of the termination of the PML on its overall performance and single out the best options available.

II. Derivation of the PML Equations

Let us consider the wave equation (WE) in the time domain in a homogeneous lossy medium governing the behavior of the vector potential $\vec{A}$ [9]:

$$\nabla^2\vec{A}-\mu\varepsilon\frac{\partial^2\vec{A}}{\partial t^2}-(\sigma_m\varepsilon+\mu\sigma)\frac{\partial\vec{A}}{\partial t}-\sigma\sigma_m\vec{A}=-\mu\vec{J} \quad (1)$$

where σ and σ_m denote the specific electric and magnetic conductivities, respectively. The equation for the electric vector potential $\vec{F}$ is the same, except for the source term $\mu\vec{J}$, which is replaced by $\varepsilon\vec{J}_m$, with $\vec{J}_m$ being the magnetic current density. In the discussion to follow, the $\vec{A}$ (1) is used as a basis for all derivations; however, all results are fully applicable to the $\vec{F}$ equation as well. Using the stretched coordinate approach [16], we introduce the complex variables s_x, s_y, s_z along the three Cartesian coordinates in the Laplacian:

$$\nabla_s^2=\frac{1}{s_x}\frac{\partial}{\partial x}\left(\frac{1}{s_x}\frac{\partial}{\partial x}\right)+\frac{1}{s_y}\frac{\partial}{\partial y}\left(\frac{1}{s_y}\frac{\partial}{\partial y}\right)+\frac{1}{s_z}\frac{\partial}{\partial z}\left(\frac{1}{s_z}\frac{\partial}{\partial z}\right) \quad (2)$$

where $s_\xi=\alpha_\xi+\sigma_\xi/(j\omega\varepsilon)$, $\xi=x,y,z$. The WE in (1) is then mapped into the frequency domain

$$\nabla_s^2\tilde{\vec{A}}-\mu\varepsilon\,(j\omega)^2\,\tilde{\vec{A}}-(\mu\sigma+\varepsilon\sigma_m)j\omega\tilde{\vec{A}}-\sigma\sigma_m\tilde{\vec{A}}=-\mu\tilde{\vec{J}}. \quad (3)$$

Six auxiliary variables are introduced in a fashion similar to that in [15]:

$$\begin{aligned}
j\omega\tilde{\vec{X}}_1&=\frac{1}{s_x}\frac{\partial\tilde{\vec{A}}}{\partial x};\quad j\omega\tilde{\vec{X}}_2=\frac{1}{s_x}\frac{\partial\left(j\omega\tilde{\vec{X}}_1\right)}{\partial x}\\
j\omega\tilde{\vec{Y}}_1&=\frac{1}{s_y}\frac{\partial\tilde{\vec{A}}}{\partial y};\quad j\omega\tilde{\vec{Y}}_2=\frac{1}{s_y}\frac{\partial\left(j\omega\tilde{\vec{Y}}_1\right)}{\partial y}\\
j\omega\tilde{\vec{Z}}_1&=\frac{1}{s_z}\frac{\partial\tilde{\vec{A}}}{\partial z};\quad j\omega\tilde{\vec{Z}}_2=\frac{1}{s_z}\frac{\partial\left(j\omega\tilde{\vec{Z}}_1\right)}{\partial z}
\end{aligned} \quad (4)$$

The mapped frequency-domain WE now becomes

$$\mu\varepsilon(j\omega)^2\tilde{\vec{A}}+(\mu\sigma+\varepsilon\sigma_m)j\omega\tilde{\vec{A}}+\sigma\sigma_m\tilde{\vec{A}}=j\omega\tilde{\vec{X}}_2+j\omega\tilde{\vec{Y}}_2+j\omega\tilde{\vec{Z}}_2+\mu\tilde{\vec{J}} \quad (5)$$

which can be mapped back into the time domain as

$$\mu\varepsilon\frac{\partial^2\vec{A}}{\partial t^2}+(\varepsilon\sigma_m+\mu\sigma)\frac{\partial\vec{A}}{\partial t}+\sigma\sigma_m\vec{A}=\frac{\partial\vec{X}_2}{\partial t}+\frac{\partial\vec{Y}_2}{\partial t}+\frac{\partial\vec{Z}_2}{\partial t}+\mu\vec{J}. \quad (6)$$

The auxiliary variables in the time domain are calculated according to the equations in (4), which are also mapped back into the time domain

$$\begin{aligned}
\alpha_x\frac{\partial\vec{X}_1}{\partial t}+\frac{\sigma_x}{\varepsilon}\vec{X}_1&=\frac{\partial\vec{A}}{\partial x};\quad \alpha_x\frac{\partial\vec{X}_2}{\partial t}+\frac{\sigma_x}{\varepsilon}\vec{X}_2=\frac{\partial^2\vec{X}_1}{\partial x\partial t}\\
\alpha_y\frac{\partial\vec{Y}_1}{\partial t}+\frac{\sigma_y}{\varepsilon}\vec{Y}_1&=\frac{\partial\vec{A}}{\partial y};\quad \alpha_y\frac{\partial\vec{Y}_2}{\partial t}+\frac{\sigma_y}{\varepsilon}\vec{Y}_2=\frac{\partial^2\vec{Y}_1}{\partial y\partial t}\\
\alpha_z\frac{\partial\vec{Z}_1}{\partial t}+\frac{\sigma_z}{\varepsilon}\vec{Z}_1&=\frac{\partial\vec{A}}{\partial z};\quad \alpha_z\frac{\partial\vec{Z}_2}{\partial t}+\frac{\sigma_z}{\varepsilon}\vec{Z}_2=\frac{\partial^2\vec{Z}_1}{\partial z\partial t}.
\end{aligned} \quad (7)$$

Equations (6) and (7) are the basis of the proposed 3-D wave equation PML ABC.

A slight modification of (6) and (7) is needed when a dielectric/magnetic interface intersects the PML medium. Suppose a dielectric interface of unit normal $\hat{n}=\hat{z}$ terminates in the PML absorber. The A_z potential governing equation then becomes [9]

$$\nabla_z^2A_z-\mu\varepsilon\frac{\partial^2A_z}{\partial t^2}-(\sigma_m\varepsilon+\mu\sigma)\frac{\partial A_z}{\partial t}-\sigma\sigma_mA_z=-\mu J_z \quad (8)$$

where the modified Laplacian ∇_x^2 is defined as

$$\nabla_z^2=\frac{\partial^2}{\partial x^2}+\frac{\partial^2}{\partial y^2}+\varepsilon_r\frac{\partial}{\partial z}\left(\frac{1}{\varepsilon_r}\frac{\partial}{\partial z}\right). \quad (9)$$

Here, ε_r denotes the local relative dielectric permittivity at the point where the respective derivative is calculated. As a result, the stretched-coordinate [16] Laplacian of (2) is now defined as

$$\nabla_{sz}^2=\frac{1}{s_x}\frac{\partial}{\partial x}\left(\frac{1}{s_x}\frac{\partial}{\partial x}\right)+\frac{1}{s_y}\frac{\partial}{\partial y}\left(\frac{1}{s_y}\frac{\partial}{\partial y}\right)+\frac{\varepsilon_r}{s_z}\frac{\partial}{\partial z}\left(\frac{1}{\varepsilon_r}\frac{\partial}{\partial z}\right). \quad (10)$$

The modification of the auxiliary variables can be easily derived thereafter.

III. Discretization

All the equations are discretized using central finite differences. The auxiliary variables $\vec{X}_1$, $\vec{Y}_1$ and $\vec{Z}_1$ are positioned half a cell "after" the locations of $\vec{A}$ in the direction of the x-, y-, and z-axis, respectively; and $\vec{X}_2$, $\vec{Y}_2$, $\vec{Z}_2$ are at the same locations as $\vec{A}$ (see Fig. 1). For stability purposes, the auxiliary variables are normalized and the following quantities are actually calculated

$$\begin{aligned}
\vec{x}_1&=\vec{X}_1\frac{\Delta l_{\min}}{\Delta t};\quad \vec{x}_2=\vec{X}_2\frac{\Delta l_{\min}^2}{\Delta t}\\
\vec{y}_1&=\vec{Y}_1\frac{\Delta l_{\min}}{\Delta t};\quad \vec{y}_2=\vec{Y}_2\frac{\Delta l_{\min}^2}{\Delta t}\\
\vec{z}_1&=\vec{Z}_1\frac{\Delta l_{\min}}{\Delta t};\quad \vec{z}_2=\vec{Z}_2\frac{\Delta l_{\min}^2}{\Delta t}.
\end{aligned} \quad (11)$$

Here

$$\Delta l_{\min}=\min_{\substack{1\le i\le n_{x\max}\\1\le j\le n_{y\max}\\1\le k\le n_{z\max}}}(\Delta x(i),\Delta y(j),\Delta z(k)) \quad (12)$$

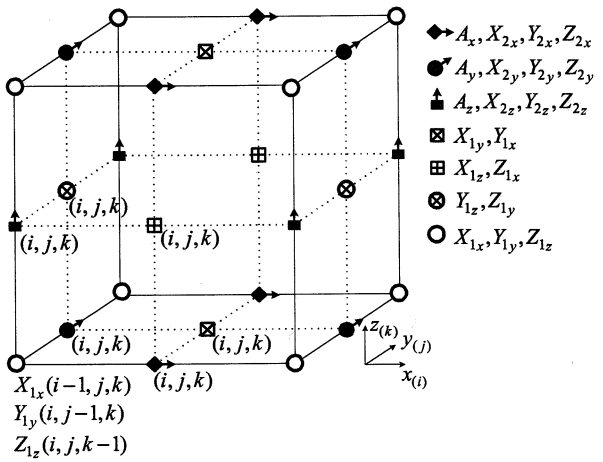

Fig. 1. Discretization cell showing the spatial location of the components of the vector potential and the corresponding auxiliary variables.

is the minimal spatial step in the nonuniform grid. The time step Δt must be chosen such that Courant's stability condition is satisfied. In our applications, it is set to $\Delta t = \Delta l_{\min}/(2c)$ where c is the highest velocity of light in the analyzed structure. Thus the spatial increments can be expressed through the dimensionless coefficients $h_x(i)$, $h_y(j)$, $h_z(k)$ as

$$\begin{aligned}
\Delta x(i) =& h_x(i)\Delta l_{\min}; \quad h_x(i) \geq 1, \quad 1 \leq i \leq n_{x\max} \\
\Delta y(j) =& h_y(j)\Delta l_{\min}; \quad h_y(j) \geq 1, \quad 1 \leq j \leq n_{y\max} \\
\Delta z(k) =& h_z(k)\Delta l_{\min}; \\
& h_z(k) \geq 1, \quad 1 \leq k \leq n_{z\max}.
\end{aligned} \tag{13}$$

Since, in general, $\vec{A} = A_x\hat{x} + A_y\hat{y} + A_z\hat{z}$, there may be three scalar WEs for the three Cartesian components of $\vec{A}$.

We will demonstrate the discretization of the PML (6) and (7) using the A_z potential. The auxiliary variables have also their corresponding z-components: X_{1z}, Y_{1z}, Z_{1z}, X_{2z}, Y_{2z}, Z_{2z}. Let us introduce the numerical constants

$$r_\xi = \frac{\sigma_\xi \Delta t}{2\varepsilon\alpha_\xi}, \quad \xi = x, y, z. \tag{14}$$

The equations for the calculation of the normalized auxiliary variables are obtained using central differences and averaging with respect to time as shown

$$\begin{aligned}
x_{1z}^{(n+1/2)}(i,j,k) =& \left(\frac{1-r_x}{1+r_x}\right) x_{1z}^{(n-1/2)}(i,j,k) \\
&+ \frac{1}{(1+r_x)\,\alpha_x h_x(i)} \\
&\times \left[A_z^{(n)}(i+1,j,k) - A_z^{(n)}(i,j,k)\right]
\end{aligned} \tag{15}$$

$$\begin{aligned}
y_{1z}^{(n+1/2)}(i,j,k) =& \left(\frac{1-r_y}{1+r_y}\right) y_{1z}^{(n-1/2)}(i,j,k) \\
&+ \frac{1}{(1+r_y)\,\alpha_y h_y(j)} \\
&\times \left[A_z^{(n)}(i,j+1,k) - A_z^{(n)}(i,j,k)\right]
\end{aligned} \tag{16}$$

$$\begin{aligned}
z_{1z}^{(n+1/2)}(i,j,k) =& \left(\frac{1-r_z}{1+r_z}\right) z_{1z}^{(n-1/2)}(i,j,k) \\
&+ \frac{1}{(1+r_z)\,\alpha_z h_z(k)} \\
&\times \left[A_z^{(n)}(i,j,k+1) - A_z^{(n)}(i,j,k)\right]
\end{aligned} \tag{17}$$

$$\begin{aligned}
x_{2z}^{(n+1/2)}(i,j,k) =& \left(\frac{1-r_x}{1+r_x}\right) x_{2z}^{(n-1/2)}(i,j,k) \\
&+ \frac{1}{(1+r_x)\,\alpha_x h_x(i-1)} \\
&\cdot \Big[x_{1z}^{(n+1/2)}(i,j,k) \\
&- x_{1z}^{(n+1/2)}(i-1,j,k) \\
&- x_{1z}^{(n-1/2)}(i,j,k) \\
&+ x_{1z}^{(n-1/2)}(i-1,j,k)\Big]
\end{aligned} \tag{18}$$

$$\begin{aligned}
y_{2z}^{(n+1/2)}(i,j,k) =& \left(\frac{1-r_y}{1+r_y}\right) y_{2z}^{(n+1/2)}(i,j,k) \\
&+ \frac{1}{(1+r_y)\,\alpha_y h_y(j-1)} \\
&\cdot \Big[y_{1z}^{(n+1/2)}(i,j,k) \\
&- y_{1z}^{(n+1/2)}(i,j-1,k) \\
&- y_{1z}^{(n-1/2)}(i,j,k) \\
&+ y_{1z}^{(n-1/2)}(i,j-1,k)\Big]
\end{aligned} \tag{19}$$

$$\begin{aligned}
z_{2z}^{(n+1/2)}(i,j,k) =& \left(\frac{1-r_z}{1+r_z}\right) z_{2z}^{(n-1/2)}(i,j,k) \\
&+ \frac{1}{(1+r_z)\,\alpha_z h_z(k-1)} \\
&\cdot \Big[z_{1z}^{(n+1/2)}(i,j,k) \\
&- z_{1z}^{(n+1/2)}(i,j,k-1) \\
&- z_{1z}^{(n-1/2)}(i,j,k) \\
&+ z_{1z}^{(n-1/2)}(i,j,k-1)\Big].
\end{aligned} \tag{20}$$

Equation (6) is discretized in a similar manner, which leads to the following finite-difference expression

$$\begin{aligned}
D_t A_z^{(n+1/2)}(i,j,k) =& \left(\frac{1-r_0}{1+r_0}\right) D_t A_z^{(n-1/2)}(i,j,k) \\
&+ \frac{1}{4\mu_r\varepsilon_r\,(1+r_0)} \\
&\cdot \left[\{A_z\} - \sigma\sigma_m \Delta l_{\min}^2 \right. \\
&\left. \cdot A_z^{(n)}(i,j,k) + l_{\min}^2 \cdot \mu J_z\right]
\end{aligned} \tag{21}$$

where

$$\begin{aligned}
\mathfrak{L}\{\mathfrak{A}_\mathfrak{z}\} =& \mathfrak{x}_{2\mathfrak{z}(\mathfrak{i},\mathfrak{j},\mathfrak{k})}^{(\mathfrak{n}+1/2)} - \mathfrak{x}_{2\mathfrak{z}(\mathfrak{i},\mathfrak{j},\mathfrak{k})}^{(\mathfrak{n}-1/2)} + \mathfrak{y}_{2\mathfrak{z}(\mathfrak{i},\mathfrak{j},\mathfrak{k})}^{(\mathfrak{n}+1/2)} \\
& - y_{2z(i,j,k)}^{(n-1/2)} + z_{2z(i,j,k)}^{(n+1/2)} - z_{2z(i,j,k)}^{(n-1/2)}
\end{aligned} \tag{22}$$

is the analog of the finite-difference Laplacian operator applied to A_z. The numerical constant

$$r_0 = \frac{\Delta t}{2}\left(\frac{\sigma_m}{\mu} + \frac{\sigma}{\varepsilon}\right) \tag{23}$$

is introduced in (21) for convenience; and, D_t is a first-order finite-difference operator in time such that

$$D_t A_z^{(n+1/2)}(i,j,k) = A_z^{(n+1)}(i,j,k) - A_z^{(n)}(i,j,k). \tag{24}$$

In a finite-difference second-order algorithm, the time-derivative of a potential function (e.g., $D_t A_z$) requires storage in addition to the storage of the function value (e.g., A_z). It should be pointed out that sources are unlikely to exist in a practical PML region and, therefore, the term μJ_z in (21) is set to zero. Note also that the EM material constants σ, σ_m, $\varepsilon = \varepsilon_0\varepsilon_r$ and $\mu = \mu_0\mu_r$ are those of the analyzed volume terminated with the PML; in other words, they are not associated with the anisotropic PML constants defined in (14).

The formulas above are in a form suitable for straightforward implementation. The time-stepping algorithm for the wave equation PML is summarized here.

1. Update the auxiliary variables $x_{1\xi}$, $y_{1\xi}$, $z_{1\xi}$, $\xi = x,y,z$, according to **(15)–(17)**.
2. Update the auxiliary variables $x_{2\xi}$, $y_{2\xi}$, $z_{2\xi}$, $\xi = x,y,z$, according to **(18)–(20)**.
3. Update the time-derivatives $D_t A_\xi$, $\xi = x,y,z$, according to **(21)**.
4. Update the potential components A_ξ, $\xi = x,y,z$, using

$$A_\xi^{(n+1)}(i,j,k) = A_\xi^{(n)}(i,j,k) + D_t A_\xi^{(n+1/2)}(i,j,k). \tag{25}$$

It should be reiterated that in the TDWP algorithm [9], [10], the above procedure is applied to both the magnetic potential A_ξ and to the electric potential F_ξ.

IV. Profiles of the PML Variables

The performance of the PML absorber depends on the combined influence of its parameters: the user-defined theoretical reflection coefficient R_0, the PML conductivity σ_ξ, and the PML loss factor σ_ξ ($\xi = x,y,z$), which takes care of the evanescent mode attenuation. The last two parameters depend on the user-defined constant $\varepsilon_{\max}$ and power rate n. Initially, we have implemented a variety of profiles already available in the literature, such as in [1]. However, the PML is now integrated with the wave equation, which is a second-order PDE. The conventional PML profiles did not perform well and they had to be modified and optimized. It is well known that greater rates of attenuation can be attained by choosing larger increments in the values of the PML parameters σ_ξ and α_ξ. Larger attenuation means decreased thickness of the PML absorber, and, therefore, less computational load. However, a larger attenuation rate gives rise to spurious numerical reflections. A compromise must be reached between insufficient and excessive attenuation. It has been observed that the first few PMLs cause the greatest numerical reflections (due to the stepwise PML conductivity jumps in the discrete space). That is why the increments in the conductivity in the first few PMLs have to be small. However, in order to reach sufficient attenuation, the PML conductivity has to increase significantly toward the final layer. If one needs a broadband performance, the rate of attenuation has to be decreased in comparison with the case of the narrow-band requirements. The number of PMLs is in direct relation with the rate of conductivity increase. The slower the conductivity rises, the thicker the absorber must be to ensure broadband performance.

Many papers are devoted to the optimization of the performance of the PML absorbers. Some of them concern frequency-domain applications [19]; others concern FDTD applications[21]. Neither of them optimizes all PML parameters simultaneously because of the complexity of the problem. In fact, all of them optimize one or two parameters. Our initial attempt to use and optimize the conductivity profile as proposed in [23] did not give satisfactory results for the wave equation in the time domain. The objective of this work was to find a problem-independent PML absorber for broad frequency band applications. This is achieved by a new degree of freedom in the definition of the PML parameters: the PML conductivity profile and the PML loss factor are allowed to increase at different power rates. We have found that the best performance is achieved when the PML conductivity σ_ξ is of one to two orders higher than the order of the PML loss factor α_ξ

$$\begin{aligned} \sigma_\xi(\rho) &= \sigma_{\max}\left(\frac{\rho}{\delta_\xi}\right)^{n+\beta}, \quad \beta \in [1,2] \\ \xi &= x,y,z \end{aligned} \tag{26}$$

$$\begin{aligned} \alpha_\xi(\rho) &= 1 + \varepsilon_{\max}\left(\frac{\rho}{\delta_\xi}\right)^{n}, \quad \rho \in [0,\delta] \\ \varepsilon &= x,y,z. \end{aligned} \tag{27}$$

Here, δ_ξ is the PML thickness in the ξ-direction, ρ is the depth in PML, R_0 is the chosen reflection coefficient at normal incidence, n is the order, and $\varepsilon_{\max}$ is a chosen constant, generally between 0 and 5. The constant β determines the order increase for σ_ξ over that indicated by n. Since the theoretical reflection coefficient at normal incidence is [1]:

$$R_0 = \exp\left(-\frac{2}{\varepsilon_0\varepsilon_r c}\int_0^\delta \sigma(\rho)d\rho\right) \tag{28}$$

one can easily obtain the PML conductivity parameter $\sigma_{\max}$ as a function of the user defined R_0

$$\sigma_{\max} = \frac{(n+\beta+1)\varepsilon_0\varepsilon_r c \ln\left(R_0^{-1}\right)}{2\delta}, \quad \beta \in [1,2]. \tag{29}$$

Increasing the power rate of the PML conductivity σ_ξ by one ($\beta = 1$), while keeping the power rate of σ_ξ the same, has the effect of broadening the frequency band in which the reflections are below -60 dB. An increase in the power rate of σ_ξ by two ($\beta = 2$) reduces the number of PMLs by additional 4 or 5 cells while the reflections can be still kept at the prescribed level, usually below -60 dB. Note that a simple increase in the

power rate n of both σ_ξ and α_ξ, as it is done in most PML absorbers, does not improve the bandwidth. It has the effect of increasing the spurious numerical reflections, thereby degrading the absorber's performance. An extensive comparison between the proposed PML variable profile and the conventional PML profiles is provided in Section VI.

V. PML Terminations

Yet another means to improve the PML performance is to replace the PEC wall that usually terminates the PML medium, with a low-cost simple ABC, which will be referred to as a single-layer ABC. In this work, three types of single-layer absorbers have been tried out to terminate the perfectly matched layer. First, the lossy one-way wave equation first-order ABC was implemented. The improvement of PML absorbers with this termination was first reported by Rappaport *et al.* [25]. Second, we have developed a lossy version of Mur's second-order ABC [26] to be used as an efficient PML termination. The third PML termination that we have developed and investigated is a lossy version of the second-order dispersive boundary condition (DBC) [27]. The choice of these termination layers has been dictated by the following considerations: the simplicity of implementation, the minimal additional computational overhead, and the fact that there are no additional memory requirements.

Here, we will describe a unified approach to the derivation of lossy PML terminations from existing single-layer ABCs, which were originally designed to terminate loss-free computational domains. The EM potential wave (1) inside the PML region has its EM constitutive parameters such that they must satisfy the constraint for reflection-free propagation

$$\frac{\sigma}{\varepsilon} = \frac{\sigma_m}{\mu} = \frac{1}{\tau} \tag{30}$$

where τ is the dielectric (and magnetic) relaxation constant. Having in mind (30), (1) can be written in the factored form

$$\left(L^2 - \mu\varepsilon\nabla^2\right)\left\{\vec{A}\right\} = 0 \tag{31}$$

where $L = \partial/\partial t + \tau^{-1}$. In (31), it is implied that there are no sources present in the PML region. Equation (31) is the basis for all first and second order lossy ABCs considered here.

In the direction of propagation (absorption), say ξ-direction ($\xi = x, y, z$), the 1-D version of (31) is

$$L^+L^-\{\vec{A}\} = 0 \tag{32}$$

where the wave operators L^+ and L^- are defined as

$$L^+ = L + \frac{v_\xi \partial}{\partial \xi} \tag{33}$$

$$L_- = L - \frac{v_\xi \partial}{\partial \xi}. \tag{34}$$

Here, v_ξ is the velocity of propagation in the ξ-direction. Taking only the operator in (33), which describes the forward (one-way) propagating wave, one obtains the lossy one-way wave equation ABC [25]

$$\frac{1}{v_\xi}\left(\frac{\partial \vec{A}}{\partial t} + \frac{\vec{A}}{\tau}\right) + \frac{\partial \vec{A}}{\partial \xi} = 0. \tag{35}$$

To derive the lossy version of Mur's second-order ABC, we follow the general procedure given in [26] while substituting the $\partial/\partial t$ derivative by the operator $(\partial/\partial t + \tau^{-1})$ in (31). Thus, this termination is obtained as

$$\frac{\partial^2 \vec{A}}{\partial t^2} = -\frac{2}{\tau}\frac{\partial \vec{A}}{\partial t} - v\frac{\partial^2 \vec{A}}{\partial \xi \partial t} - \frac{v}{\tau}\frac{\partial \vec{A}}{\partial x} - \frac{1}{\tau^2}\vec{A} + \frac{v^2}{2}\left(\frac{\partial^2 \vec{A}}{\partial \eta^2} + \frac{\partial^2 \vec{A}}{\partial \zeta^2}\right) \tag{36}$$

where $v = (\mu\varepsilon)^{-1/2}$, and (η, ζ) are the transverse with respect to ξ coordinates.

Similarly, from the original second-order DBC [27]

$$\left(\frac{1}{v_{1\xi}}\frac{\partial}{\partial t} + \frac{\partial}{\partial \xi}\right)\left(\frac{1}{v_{2\xi}}\frac{\partial}{\partial t} + \frac{\partial}{\partial \xi}\right)\{\vec{A}\} = 0 \tag{37}$$

its lossy version is obtained as follows:

$$\left[\frac{1}{v_{1\xi}}\left(\frac{\partial}{\partial t} + \frac{1}{\tau}\right) + \frac{\partial}{\partial \xi}\right]\left[\frac{1}{v_{2\xi}}\left(\frac{\partial}{\partial t} + \frac{1}{\tau}\right) + \frac{\partial}{\partial \xi}\right]\{\vec{A}\} = 0 \tag{38}$$

where $v_{1\xi}$ and $v_{2\xi}$ are the velocities in the direction of propagation (absorption), corresponding to two different frequencies in the band of interest.

The discretizations of (35), (36), and (38) are given in the Appendix.

VI. Numerical Results and Discussion

To validate the method, we have applied this PML ABC to both radiation and waveguide problems solved in terms of wave potentials in the time domain. Here, we will consider two structures: a dipole in open space, and a rectangular waveguide partially filled with dielectric. The problem of the z-directed infinitesimal dipole, which radiates in open space, has two planes of symmetry. Therefore, the computational domain can be only the first octant whose dimensions are $(60\Delta x, 60\Delta y, 60\Delta z)$, where $\Delta x = \Delta y = \Delta z = 2.5$ mm. The potential A_z is excited by the z-directed current of the dipole, which is a Gaussian pulse in time. The reflection is estimated using the ratio of reflected and incident wave potential, which in this case is the z-component of the magnetic vector potential $\vec{A} = \hat{z}A_z$

$$R_{\mathrm{dB}} = 20\log_{10}\left|\frac{\mathfrak{F}\{A_z^{\mathrm{refl}}\}}{\mathfrak{F}\{A_z^{\mathrm{inc}}\}}\right| \tag{39}$$

Here, $\mathfrak{F}$ denotes the Fourier transform of the respective time-dependent potential. It should be noted that the reflections can be calculated through the reflected and incident field quantities as well. The results are identical to those obtained from the potentials in (39).

We investigate three types of PML ABCs to terminate the computational domain of the time-domain wave equation. They have different variable profiles. The first type implements the

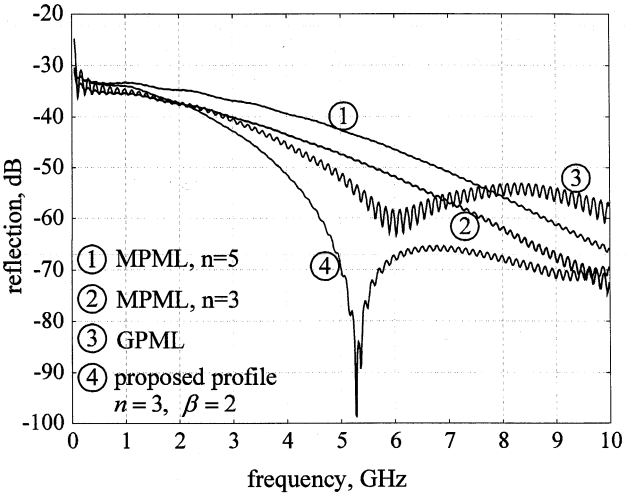

Fig. 2. Spectrum of the reflection in the dipole radiation problem using three different PML conductivity profiles; $N_{\rm PML} = 16$, $R_0 = 10^{-3}$, $\varepsilon_{\max} = 3$ in all four cases.

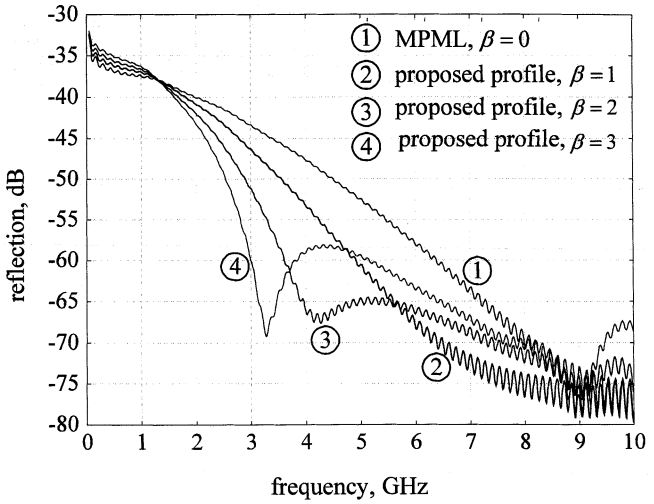

Fig. 3. Dependence of the spectrum bandwidth of the reflection in the dipole radiation problem on the PML conductivity parameter β; $n = 3$, $N_{\rm PML} = 20$, $R_0 = 10^{-4}$, $\varepsilon_{\max} = 4$ in all cases.

MPML conductivity profiles as in [17]. The performance of two MPML profiles is shown in Fig. 2: for the orders $n = 3$ and $n = 5$. The second one uses the GPML profile [18]. The third absorber is based on the proposed profile as described by (26) and (27), when the orders n and β are set as: $n = 3$, $\beta = 2$. All absorbers are 16 cells thick; their theoretical reflection coefficient at normal incidence is chosen to be $R_0 = 10^{-3}$; the constant $\varepsilon_{\max}$ is set as $\varepsilon_{\max} = 3$. All of them are terminated with a PEC wall. The respective reflections are plotted in Fig. 2, which shows that our modification of the PML conductivity profile has superior performance in terms of both reflection level and frequency bandwidth. It can be observed that a simple increase of the power of the MPML from $n = 3$ to $n = 5$ does not improve its absorption. In fact, it leads to a slight increase of the reflections. In all cases, the observation point is in the dipole's H-plane, halfway between the dipole and the absorber. The results are similar for any other observation point.

Fig. 3 compares the performance of the proposed PML absorber with the regular MPML only, while varying the value of the power increase parameter β. It is evident that the frequency band becomes wider and the reflections lower in the proposed PML when its power order is increased by $\beta = 1$ or by $\beta = 2$ in comparison with the regular MPML profile, which in fact corresponds to the case of $\beta = 0$ in (26). From our experiments so far, we can draw the conclusion that the value of $\beta = 2$ provides optimal PML performance.

Fig. 4 shows the dependence of the frequency bandwidth on the number of cells in the proposed 3-D PML absorber terminating the dipole computational region. Here, it is important to point out that the physical thickness of the absorber, as a percentage of the wavelength, is very important at the lower frequency end. Generally, we can recommend a thickness of the PML medium of at least 65–70% of the longest wavelength of interest.

The rectangular waveguide has a cross section of 40 mm by 18 mm. It is half-filled with a dielectric layer parallel to its wide side (the dielectric constant is $\varepsilon_r = 2.45$). Its geometry is seen in Fig. 5. It is excited by a 4.7 GHz sine waveform modulated

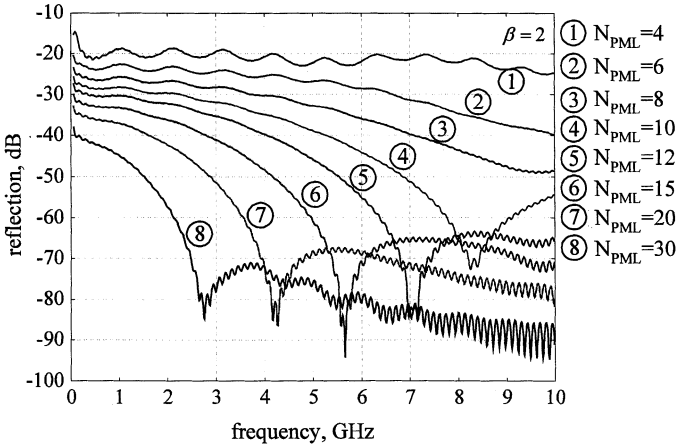

Fig. 4. Dependence of the spectrum bandwidth in the dipole radiation problem on the number of cells in the PML absorber; $R_0 = 10^{-3}$, $\varepsilon_{\max} = 3$, $n = 3$, $\beta = 2$ in all cases.

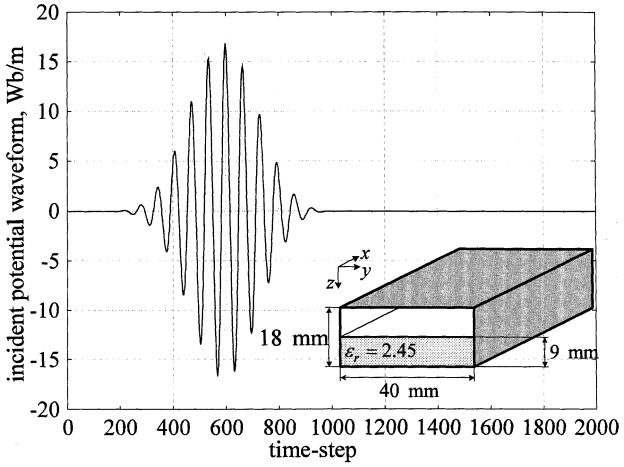

Fig. 5. Time sample of the incident potential in the partially filled rectangular waveguide, which is exciting the structure in the frequency band from 3.9 GHz to 5.5 GHz.

by Blackman-Harris window function [29], shown in Fig. 5. The time-domain sample of the reflections is given in Fig. 6 for the

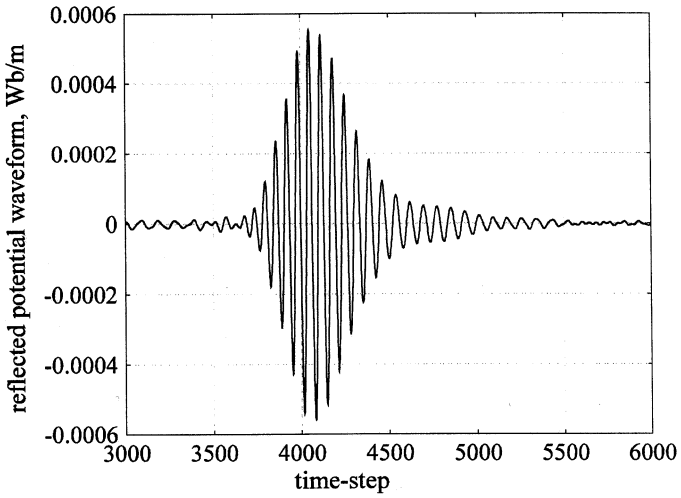

Fig. 6. Time sample of the reflected potential in the partially filled rectangular waveguide ($N_{\mathrm{PML}} = 12$, $R_0 = 10^{-5}$, $\varepsilon_{\max} = 1$, $n = 2$).

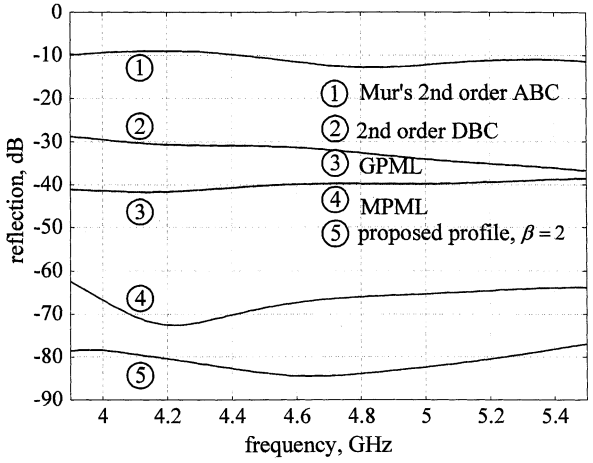

Fig. 7. Spectrum of the reflection in the waveguide problem with different ABCs; $N_{\mathrm{PML}} = 10$, $R_0 = 10^{-4}$, $\varepsilon_{\max} = 1$, $n = 2$ in all PML cases.

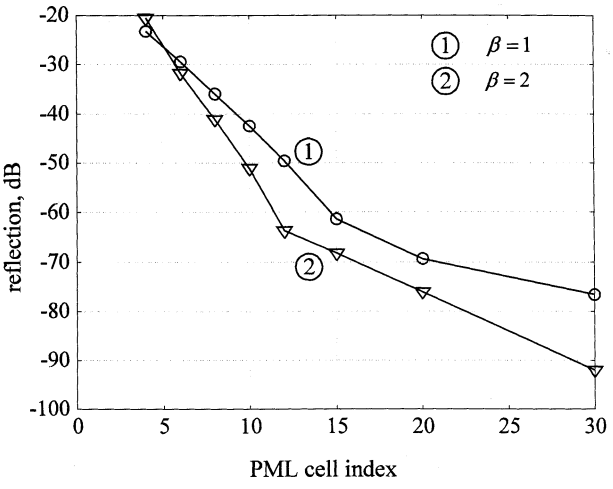

Fig. 8. Dependence of the reflection on the thickness of the PML in the dipole problem at $f = 7$ GHz for $\beta = 1$ and $\beta = 2$ ($R_0 = 10^{-4}$, $\varepsilon_{\max} = 4$, $n = 3$).

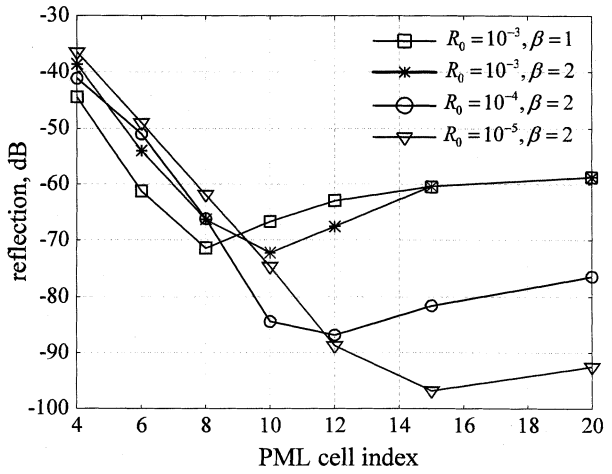

Fig. 9. Dependence of the reflection on the thickness of the PML in the partially filled waveguide at $f = 4.7$ GHz ($\varepsilon_{\max} = 1$, $n = 2$) for different theoretical reflection coefficients.

case of twelve-cell thick PML with $R^0 = 10^{-5}$, $\varepsilon_{\max} = 1, n = 2, \beta = 2$. The band-limited excitation of the waveguide has its spectrum in the frequency band from 3.9 GHz to 5.5 GHz. The transverse profile of the excitation corresponds to the dominant TM_{z10} mode, which requires a magnetic vector potential $\vec{A}$ with a z-component only [29]. The size of the computational domain is $(500\Delta x, 20\Delta y, 10\Delta z)$, where $\Delta x = \Delta y = \Delta z = 2$ mm.

To compare the performance of various absorbers with the proposed PML in a typical waveguide port termination problem, the reflection as defined in (39) was computed for five types of ABCs. The first two are single-layer absorbers: Mur's second order ABC [26], and the second-order dispersive boundary condition (DBC) [27]. The other three are PML ABCs and they are the same as those used in the case of the dipole: GPML [18], MPML [17], and the proposed new PML profile. All three PML absorbers have the following common parameters: the thickness is 10 cells, $R_0 = 10^{-4}$, $\varepsilon_{\max} = 1$, $n = 2$, their PML termination is a one-way lossy wave equation. The results are plotted in Fig. 7. The superior performance of the PML absorbers over the single-layer ABC's is obvious. Of all PML absorbers, the proposed modification in the PML profile results in the lowest reflections in the frequency band of the excitation pulse.

The dependence of the reflection level on the number of layers in the absorber was investigated for both the dipole and the waveguide problem. The purpose was to come up with a recommendation for the minimum number of layers in the absorber, which would ensure a reflection level below -60 dB dB in the frequency band of the excitation. Fig. 8 shows this dependence in the 3-D PML absorber of the dipole radiation example at $f = 7$ GHz when $R_0 = 10^{-4}$, $\varepsilon_{\max} = 4$, $n = 3$ for $\beta = 1$ and $\beta = 2$. In Fig. 9, the dependence of the reflection on the PML thickness in the waveguide port termination is shown at the central excitation frequency of 4.7 GHz, when $\varepsilon_{\max} = 1$, $n = 2$, and for different reflection coefficients $R_0 = 10^{-3}$, $R_0 = 10^{-4}$, $R_0 = 10^{-5}$. The curves in both examples are very representative of the reflection dependence on the PML thickness in the whole frequency band of the respective source. Generally, one can draw the conclusion that thicker PMLs are needed for the termination of the 3-D computational domain of the second-order wave equation compared to the termination

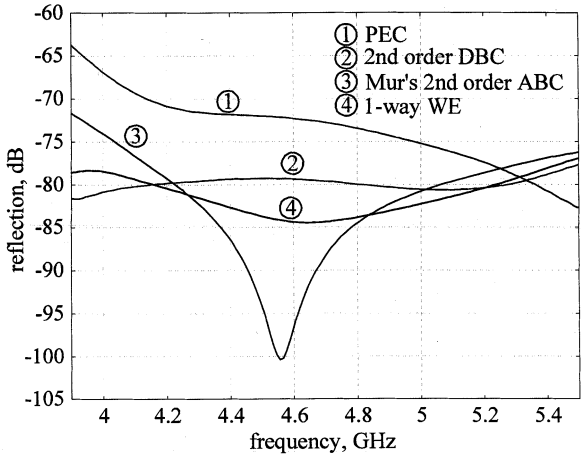

Fig. 10. Influence of the type of the termination on the PML ABC performance for the waveguide example.

of the FDTD solution of Maxwell's equations. To achieve reflections under 0.1% in a broad frequency band, at least 12 PML cells are necessary (with a PEC layer termination).

The influence of the type of termination layer on the PML performance of the PML ABC is shown in Fig. 10 where the usual termination by a PEC wall is compared to three types of lossy layer terminations: the one-way lossy WE, the lossy Mur's second-order ABC, and the lossy second order DBC. The figure shows that improvement by 5 to 15 dB is easily achievable if a single-layer lossy ABC is used instead of a PEC wall. The one-way lossy WE termination and the lossy second order DBC termination provide the desired broadband performance. It should be mentioned that the lossy DBC termination requires optimization of the two velocities $v_{1\xi}$ and $v_{2\xi}$ in (38), and there is no prescription for their choice. This is an intrinsic drawback of all DBC absorbers.

VII. Conclusion

In this paper, we propose a PML ABC for the 3-D scalar wave equation in the time domain. It is shown that the conventional PML profiles are not efficient when integrated with the second-order wave equation. Suitable low-reflection broadband PML variable profile is proposed. Its performance is verified and carefully studied in radiation and guided wave problems. The new profile handles equally well both port terminations and truncations of the computational domain of open problems. The performance of the proposed PML absorber is further improved by the use of simple single-layer ABCs to truncate the PML region. For that, the lossy version of Mur's second order ABC and the lossy version of the second order DBC have been developed and implemented. The current implementation handles inhomogeneous dielectrics intersecting the PML boundary. Further implementations include complex structures with metallic inclusions.

Appendix

Here, the discretized forms of the three single-layer PML terminations discussed in Section V will be shown in the case of $\xi = x$ for the A_ζ component of the potential, where $\zeta = x, y, z$.

1) Discretized lossy one-way WE termination in the x-direction

$$A_\zeta^{(n+1)}(i+1,j,k) = \frac{1-r_x-r_{0x}}{1+r_x} A_\zeta^{(n)}(i+1,j,k) + \frac{r_{0x}}{1+r_x} A_\zeta^{(n)}(i,j,k) \quad \text{(A.1)}$$

where

$$r_x = \frac{\sigma_x t}{2\varepsilon\alpha_x}; \quad r_{0x} = \frac{v_t}{x\sqrt{\alpha_x}}; \quad v = \frac{1}{\sqrt{\mu\varepsilon}}.$$

2) Discretized lossy Mur's second-order ABC in the x direction

$$\begin{aligned} D_t A_\zeta^{(n+1/2)}(i+1,j,k) =& \frac{1-r_{0x}}{1+r_x+r_{0x}} D_t A_\zeta^{(n-1/2)} \\ &\times (i+1,j,k) + \frac{r_{0x}}{1+r_x+r_{0x}} \\ &\times D_t A_\zeta^{(n+1/2)}(i,j,k) \\ &- \frac{r_x r_{0x}+r_x^2}{1+r_x+r_{0x}} A_\zeta^{(n)} \\ &\times (i+1,j,k) \\ &+ \frac{r_x r_{0x}}{1+r_x+r_{0x}} A_\zeta^{(n)}(i,j,k) \\ &+ \frac{t^2 v_2}{2y^2(1+r_x+r_{0x})} \\ &\times \Big[A_\zeta^{(n)}(i+1,j+1,k) \\ &\quad -2A_\zeta^{(n)}(i+1,j,k) \\ &\quad +A_\zeta^{(n)}(i+1,j-1,k) \Big] \\ &+ \frac{t^2 v_2}{2z^2(1+r_x+r_{0x})} \\ &\times \Big[A_\zeta^{(n)}(i+1,j,k+1) \\ &\quad -2A_\zeta^{(n)}(i+1,j,k) \\ &\quad +A_\zeta^{(n)}(i+1,j,k-1) \Big]. \end{aligned} \quad \text{(A.2)}$$

The coefficients r_x and r_{0x} are the same as in (A.1). The potential itself is calculated as

$$A_\zeta^{(n+1)}(i+1,j,k) = A_\zeta^{(n)}(i+1,j,k) + D_t A_\zeta^{(n+1/2)}(i+1,j,k). \quad \text{(A.3)}$$

3) Discretized second order DBC in the x-direction.

The factored differential operator in (38) is expanded to give the following DBC equation

$$\frac{\partial^2 A_\zeta}{\partial t^2} = -\frac{2}{\tau}\frac{\partial A_\zeta}{\partial t} - (v_{1x}+v_{2x})\frac{\partial^2 A_\zeta}{\partial x \partial t} - \frac{(v_{1x}+v_{2x})}{\tau}\frac{\partial A_\zeta}{\partial x} - \frac{1}{\tau^2}A_\zeta - v_{1x}v_{2x}\frac{\partial^2 A_\zeta}{\partial x^2}. \quad \text{(A.4)}$$

The discretization of (A.4) leads to

$$\begin{aligned} D_t A_\zeta^{(n+1/2)}(i+1,j,k) =& \frac{1-r_{Dx}}{1+r_x+r_{Dx}} D_t A_\zeta^{(n-1/2)} \\ &\times (i+1,j,k) + \frac{r_{Dx}}{1+r_x+r_{Dx}} \\ &\times D_t A_\zeta^{(n+1/2)}(i,j,k) \\ &- \frac{r_x r_{Dx}+r_x^2}{1+r_x+r_{Dx}} A_\zeta^{(n)} \\ &\times (i+1,j,k) + \frac{r_x r_{Dx}}{1+r_x+r_{Dx}} \\ &\times A_\zeta^{(n)}(i,j,k) \\ &+ \frac{v_{1x}v_{2x}t^2}{\alpha x^2(1+r_x+r_{Dx})} \\ &\times \Big[A_\zeta^{(n)}(i+1,j,k) \\ &\quad -2A_\zeta^{(n)}(i,j,k) \\ &\quad +A_\zeta^{(n)}(i-1,j,k)\Big] \end{aligned} \tag{A.5}$$

where

$$r_x = \frac{\sigma t}{2\varepsilon\alpha_x}; \quad r_{Dx} = \frac{(v_{1x}+v_{2x})\,t}{\Delta x\sqrt{\alpha_x}}.$$

Finally, the potential is calculated as

$$\begin{aligned} A_\zeta^{(n+1)}(i+1,j,k) =& A_\zeta^{(n)}(i+1,j,k) \\ &+ D_t A_\zeta^{(n+1/2)}(i+1,j,k). \end{aligned} \tag{A.6}$$

REFERENCES

[1] J. P. Berenger, "A perfectly matched layer for the absorption of electromagnetic waves," *J. Comput. Phys.*, vol. 114, pp. 185–200, 1994.

[2] ——, "Perfectly matched layer for the FDTD solution of wave-structure interaction problems," *IEEE Trans. Antennas Propagat.*, vol. 44, pp. 110–117, Jan. 1996.

[3] J. Tang, K. D. Paulsen, and S. A. Haider, "Perfectly matched layer mesh terminations for nodal-based finite-element methods in electromagnetic scattering," *IEEE Trans. Antennas Propagat.*, vol. 46, pp. 507–516, Apr. 1998.

[4] B. Stupfel and R. Mittra, "Numerical absorbing boundary conditions for the scalar and vector wave equations," *IEEE Trans. Antennas Propagat.*, vol. 44, pp. 1015–1022, July 1996.

[5] E. A. Marengo, C. M. Rappaport, and E. L. Miller, "Optimum PML ABC conductivity profile in FDFD," *IEEE Trans. Magn.*, vol. 35, pp. 1506–1509, May 1999.

[6] W. P. Huang, C. L. Xu, W. Lui, and K. Yokoyama, "The perfectly matched layer (PML) boundary condition for the beam propagation method," *IEEE Photon. Technol. Lett.*, vol. 8, pp. 649–651, May 1996.

[7] A. Cuccinotta, G. Pelosi, S. Selleri, L. Vincetti, and M. Zoboli, "Perfectly matched anisotropic layers for optical waveguide analysis through the finite-element beam-propagation method," *Microwave Opt. Technol. Lett.*, vol. 23, no. 2, pp. 67–69, 1999.

[8] N. Georgieva and E. Yamashita, "Time-domain vector-potential analysis of transmission line problems," *IEEE Trans. Microwave Theory Tech.*, vol. 46, pp. 404–410, Apr. 1998.

[9] N.K. Georgieva, "Construction of solutions to electromagnetic problems in terms of two collinear vector potentials," *IEEE Trans. Microwave Theory Tech.*, pp. 1950–1959, Aug. 2002.

[10] N. Georgieva and Y. Rickard, "The application of the wave potential functions to the analysis of transient electromagnetic fields," in *Proc. IEEE MTT-S Dig.*, vol. 2, June 2000, pp. 1129–1132.

[11] W. P. Huang, S. T. Chu, A. Goss, and S. K. Chaundhuri, "A scalar finite-difference time-domain approach to guided-wave optics," *IEEE Photon. Technol. Lett.*, vol. 3, pp. 524–526, June 1991.

[12] W. P. Huang, S. T. Chu, and S. K. Chaundhuri, "A semivectorial finite-difference time-domain method," *IEEE Photon. Technol. Lett.*, vol. 3, pp. 803–806, Sept. 1991.

[13] W. P. Huang, C. L. Xu, and J. Chrostowski, "A time-domain propagating scheme for simulation of dynamics of optical guided-wave devices," *IEEE Photon. Technol. Lett.*, vol. 5, pp. 1071–1073, Apr. 1993.

[14] M. Koshiba, Y. Tsuji, and M. Hikari, "Time-domain beam propagation method and its application to photonic crystal circuits," *IEEE Photon. Technol. Lett.*, vol. 18, pp. 102–110, Jan. 2000.

[15] D. Zhou, W. P. Huang, C. L. Xu, and D. G. Fang, "The perfectly matched layer boundary condition for scalar finite-difference time-domain method," *IEEE Photon. Technol. Lett.*, vol. 13, pp. 454–456, May 2001.

[16] W. C. Chew and W. H. Weedon, "A 3D perfectly matched medium from modified Maxwell's equations with stretched coordinates," *Microwave Opt. Technol. Lett.*, vol. 7, no. 13, pp. 599–604, 1994.

[17] B. Chen, D. G. Fang, and B. H. Zhou, "Modified Berenger PML absorbing boundary condition for FD-TD meshes," *IEEE Microwave Guided Wave Lett.*, vol. 5, pp. 399–401, Nov. 1995.

[18] J. Fang and Z. Wu, "Generalized perfectly matched layer for the absorption of propagating and evanescent waves in lossless and lossy media," *IEEE Trans. Microwave Theory Tech.*, vol. 44, pp. 2216–2222, Dec. 1996.

[19] D. Johnson, C. Furse, and A. Tripp, "Application and optimization of the perfectly matched layer boundary condition for geophysical simulations," *Microwave Opt. Technol. Lett.*, vol. 25, no. 4, pp. 253–55, 2000.

[20] E. Michielssen, W. C. Chew, and D. S. Weile, "Genetic algorithm optimized perfectly matched layers for finite difference frequency domain applications," in *IEEE AP-S Symp.*, 1996, pp. 2106–2109.

[21] J. S. Juntunen, N. V. Kantartzis, and T. D. Tsiboukis, "Zero reflection coefficient in discretized PML," *IEEE Microwave Wireless Comp. Lett.*, vol. 11, pp. 155–157, Apr. 2001.

[22] S. C. Winton and C. M. Rappaport, "Specifying PML conductivities by considering numerical reflection dependencies," *IEEE Trans. Antennas Propagat.*, vol. 48, pp. 1055–1063, July 2000.

[23] G. Lazzi and O. P. Gandhi, "Inversion theory as applied to the optimization of conductivity profile for PML absorbing boundary condition for FDTD code," *Electron. Lett.*, vol. 33, no. 6, pp. 502–503, 1997.

[24] ——, "On the optimal design of the PML absorbing boundary condition for the FDTD code," *IEEE Trans. Antennas Propagat.*, vol. 45, pp. 914–916, May 1997.

[25] C. M. Rappaport, "Interpreting and improving the PML absorbing boundary condition using anisotropic lossy mapping of space," *IEEE Trans. Magn.*, vol. 32, pp. 968–974, May 1996.

[26] G. Mur, "Absorbing boundary conditions for the finite-difference approximation of the time-domain electromagnetic-field equations," *IEEE Trans. Electromagn. Compat.*, vol. EMC-23, pp. 377–382, 1981.

[27] Z. Bi, K. L. Wu, C. Wu, and J. Litva, "A dispersive boundary condition for microstrip component analysis using FDTD method," *IEEE Trans. Microwave Theory Tech.*, vol. 40, pp. 774–777, May 1992.

[28] F. J. Harris, "On the use of windows for harmonic analysis with the discrete fourier transform," *Proc. IEEE*, vol. 66, pp. 51–83, 1978.

[29] R. F. Harrington, *Time-Harmonic Electromagnetic Fields*. New York: McGraw-Hill, 1961, pp. 158–161.

Yotka S. Rickard received the M.Sc. degree in mathematics and the Ph.D. degree in engineering from McMaster University, Hamilton, ON, Canada, in 1997 and 2002, respectively.

From 1984 to 1993, she was as Assistant Professor with the Institute for Applied Mathematics and Informatics, Technical University of Sofia, Bularia. Currently, she is a Postdoctoral Researcher, with the Computational Electromagnetics Laboratory, McMaster University. Her research interests include numerical solution of time-dependent partial differential equations and integral equations, and their application in computational electromagnetics and photonics.

Natalia K. Georgieva (M'97) received the Dipl. Eng. degree from the Technical University of Varna, Bulgaria, in 1989, and the Ph.D. degree from the University of Electro-Communications, Tokyo, Japan, in 1997.

From 1998 to 1999, she held a Postdoctoral Fellowship of the Natural Sciences and Engineering Research Council of Canada (NSERC), during which time she was with the Microwave and Electromagnetics Laboratory, DalTech, Dalhousie University, Halifax, Canada, and with the Simulation Optimization Systems Research Laboratory, McMaster University, Hamilton, ON, Canada. In July 1999, she joined the Department of Electrical and Computer Engineering, McMaster University, as an Assistant Professor. Her research interests includes theoretical and computational electromagnetism, high-frequency analysis techniques, as well as CAD methods for high-frequency structures and antennas.

Dr. Georgieva received the Natural Sciences and Engineering Research Council of Canada (NSERC) University Faculty Award in 2000.

Wei-Ping Huang (SM'93) received the B.S. degree in microwave engineering from Shandong University, China, in 1982 with provincial and national honors. He received the M.S. degree with specialization in fiber optics in 1984 from the University of Science and Technology of China, and the Ph.D degree in integrated optics in 1989 from the Massachusetts Institute of Technology (MIT), Cambridge. At MIT, he also studied international business management at the Sloan School of Management.

He has held a variety of faculty positions with the Engineering Department of the University of Waterloo, Waterloo, ON, Canada, and McMaster University, Hamilton, ON, Canada, including Assistant Professor, Associate Professor with tenure, and Full Professor. He has had visiting, adjunct, and consulting positions with several academic and industrial institutions in Canada, the U.S., Japan, and China. He was with Nortel from January to August 1992 and again from May to August 1993. He was a Visiting Professor with NTT Optoelectronics Lab from September 1995 to August 1996. In his capacity as the leader of the photonic research group at Waterloo and later at McMaster, he has successfully carried out a number of major research projects in a wide range of areas in fiber optics and integrated photonics, sponsored by Canadian federal/provincial governments and private companies in Canada, the United States, and Japan. He has also held a number of executive and advisory positions in a number of photonic start-up companies in Canada and the United States. He is internationally known for his contributions and expertise for photonic devices and integrated circuits. He has authored and coauthored more than 100 journal papers and 70 conference papers and holds seven United States patents.

Dr. Huang is a Member of OSA and SPIE. He was elected to the MIT Electromagnetics Academy and received the Distinguished Leadership Award from the American Biographical Institute in 1996. He was elected as a Cheung Kong Scholars by Ministry of Education, China, and Li Ka Shing Foundation, Hong Kong, in 2000.